Cobalt-Catalyzed Electrophilic Aminations with Anthranils: An Expendient Route to Condensation Quinolines**

Jie Li, Eric Tan, Niklas Keller, Yi-Hung Chen, Peter M. Zehetmaier, Andreas C. Jakowetz, Thomas Bein* and Paul Knochel**

Contents

Methods

UV-VIS-NIR spectra were recorded using a Perkin-Elmer Lambda 1050 spectrometer equipped with a 150 mm integrating sphere and photomultiplier tube (PMT) and InGaAs detectors.
Steady-state photoluminescence (PL) measurements and t**ime-correlated single photon counting** (TCSPC) measurements were performed using a PicoQuant FluoTime 300 spectrometer equipped with a 378 nm picosecond diode laser (pulse power 0.99 nJ cm^{-2}, pulse rate 40 MHz).

Cyclic voltammetry measurements were measured using 100 or 200 µM solutions of the condensed N-heterocycles in acetonitrile, with 0.2 M tetrabutylammonium hexafluorophosphate as electrolyte and 0.2 mM ferrocene as internal reference and external reference. Measurements were performed with a Metrohm Autolab PGSTAT302N potentiostat, using Pt wires as the working electrode and counter electrode and an Ag wire as reference electrode. The potential window was from −1.6 V up to 2.6 V with a scan speed of 50 mVs−1.

UV-Vis spectroscopy and photoluminescence spectroscopy

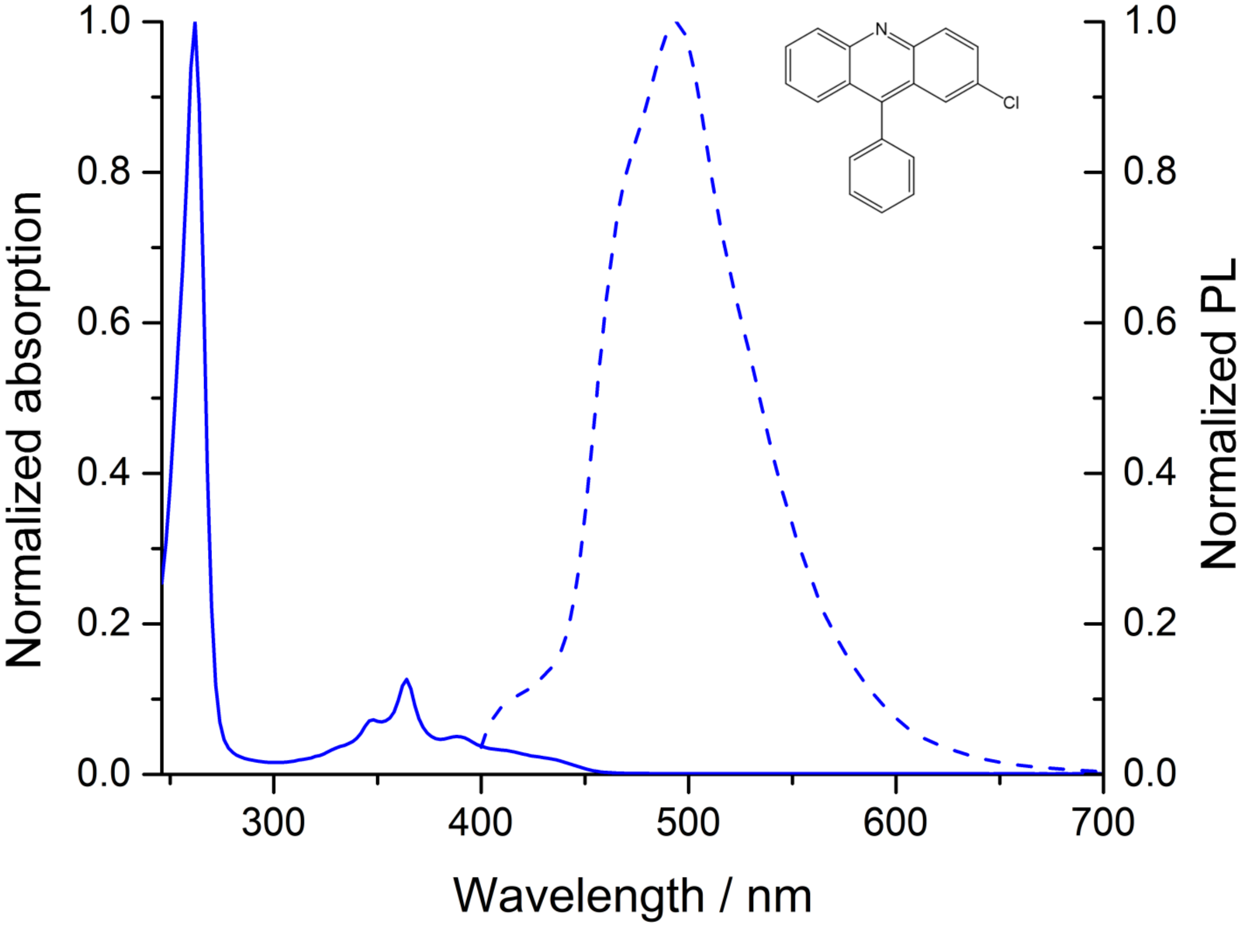

Figure 1: Normalized absorption and photoluminescence spectrum of compound **6a** in solution (50 µM in $CHCl_3$).

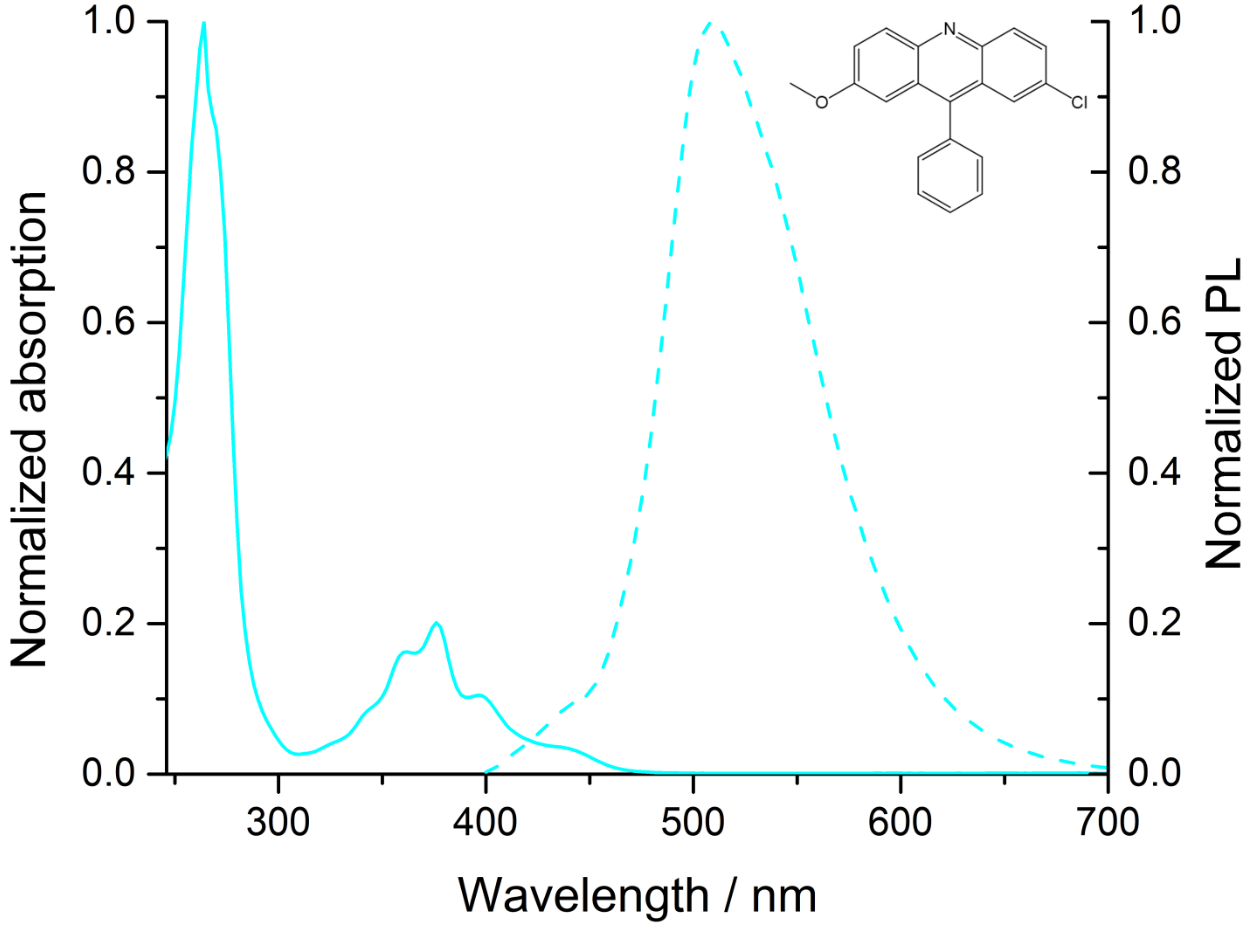

Figure 2: Normalized absorption and photoluminescence spectrum of compound **6b** in solution (50 µM in $CHCl_3$).

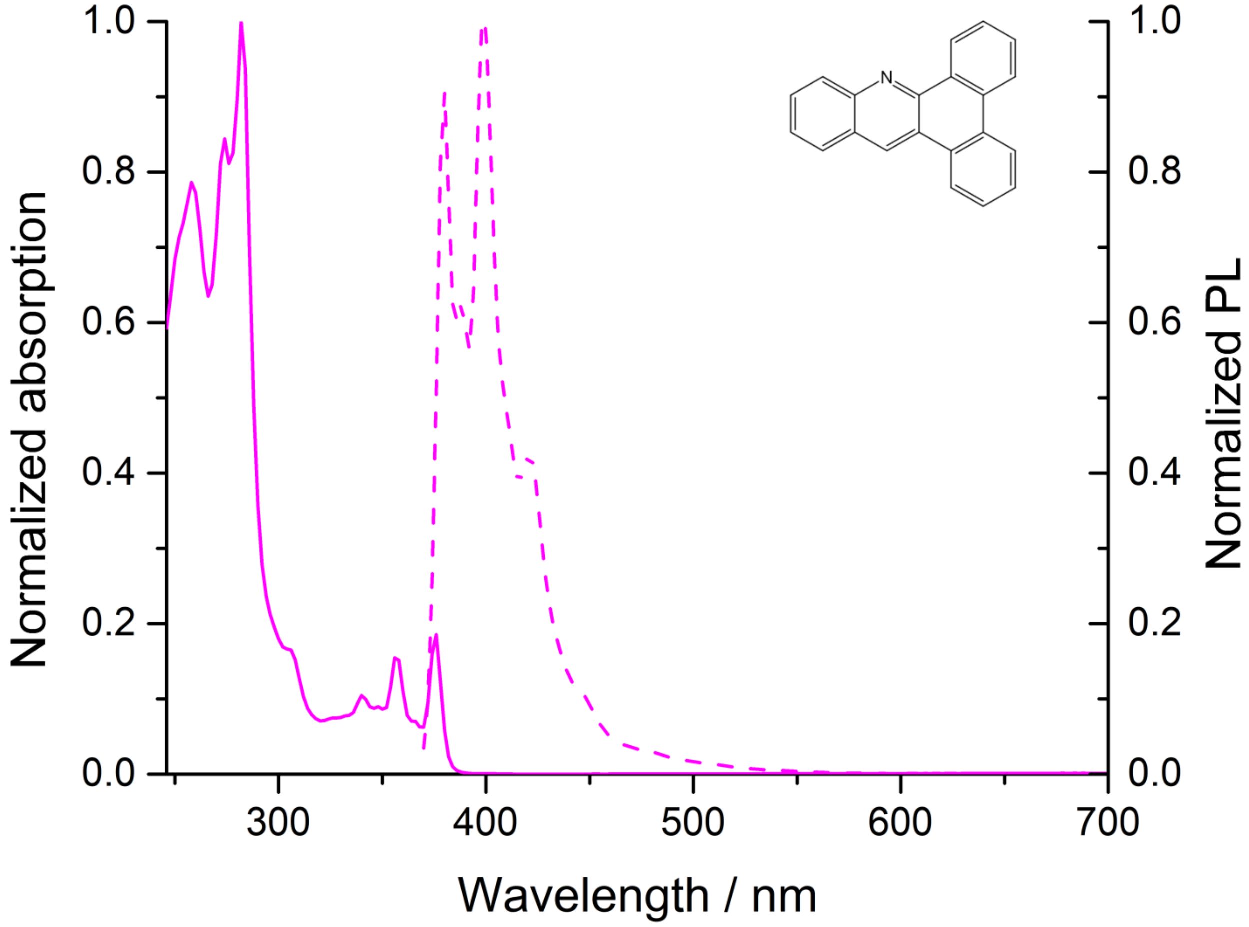

Figure 3: Normalized absorption and photoluminescence spectrum of compound **10a** in solution (50 µM in $CHCl_3$).

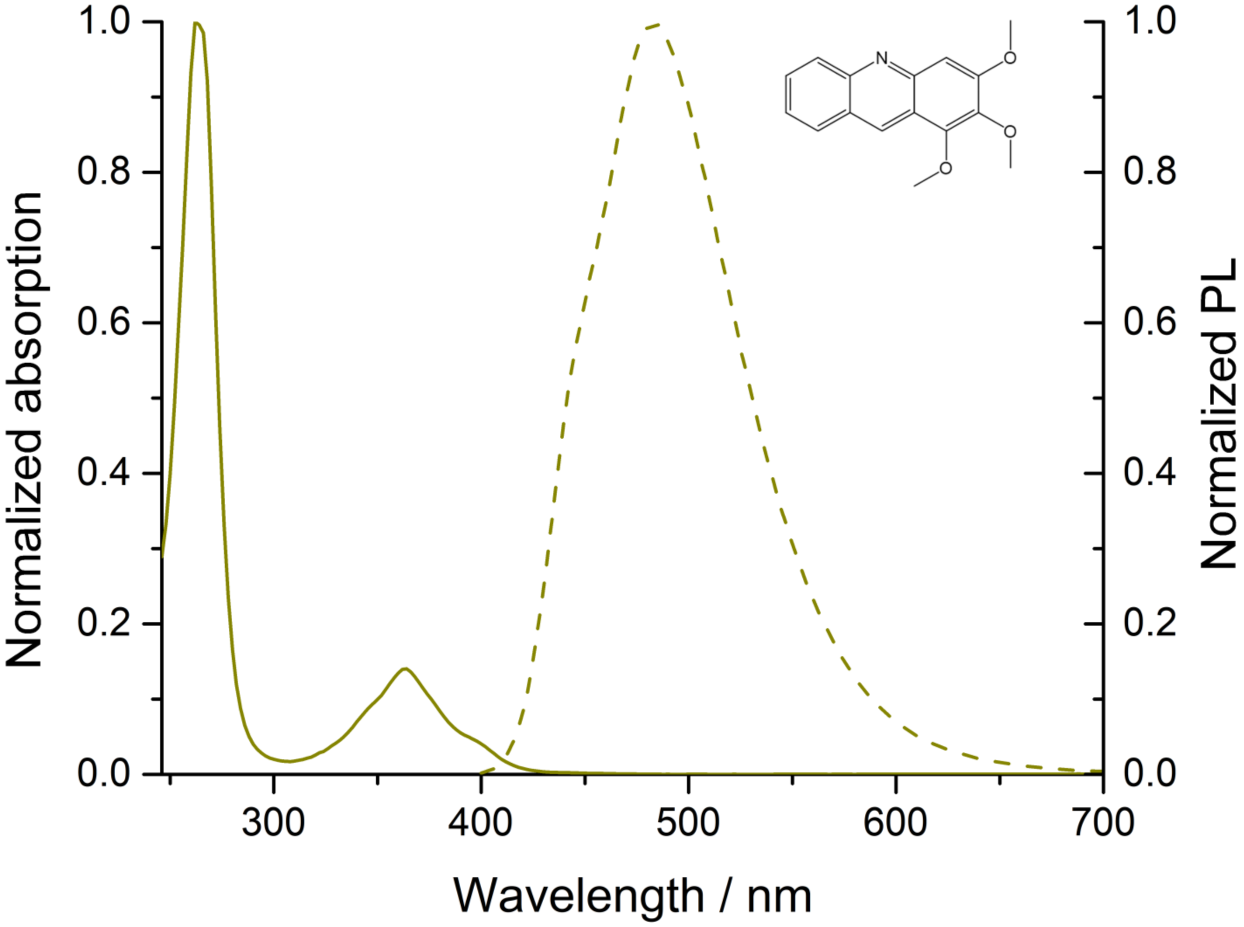

Figure 4: Normalized absorption and photoluminescence spectrum of compound **10b** in solution (50 µM in $CHCl_3$).

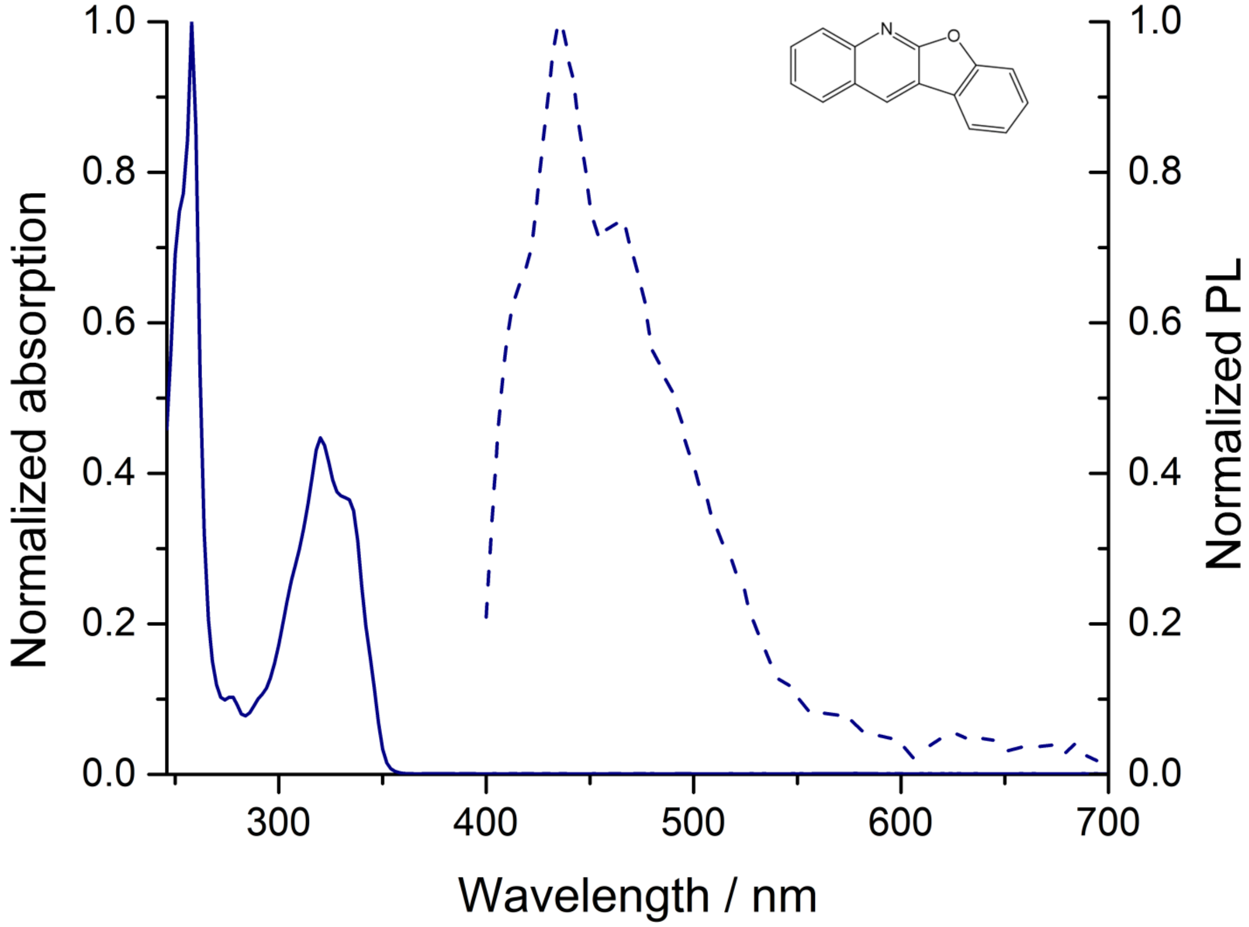

Figure 5: Normalized absorption and photoluminescence spectrum of compound **10d** in solution (50 µM in $CHCl_3$).

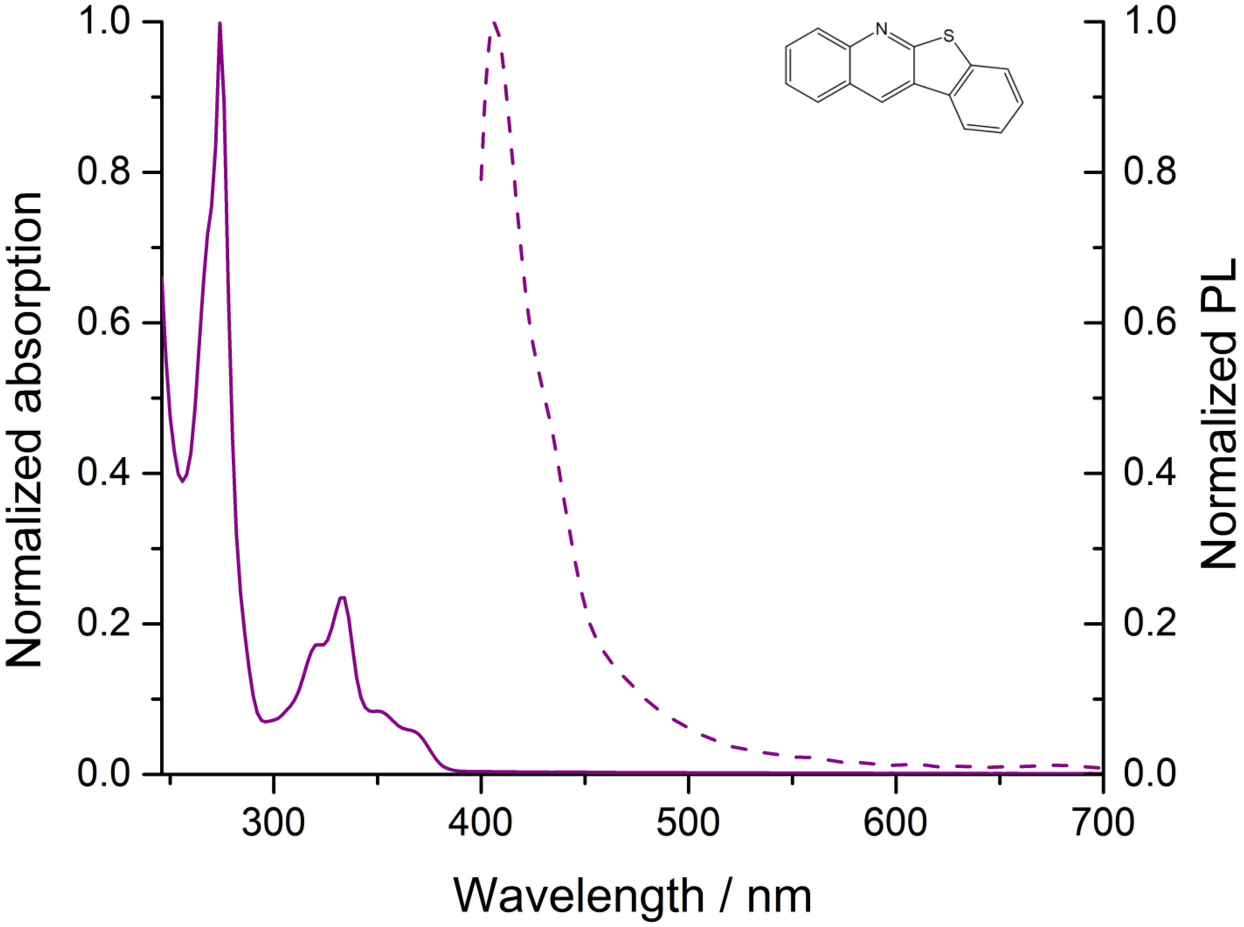

Figure 6: Normalized absorption and photoluminescence spectrum of compound **10e** in solution (50 µM in $CHCl_3$).

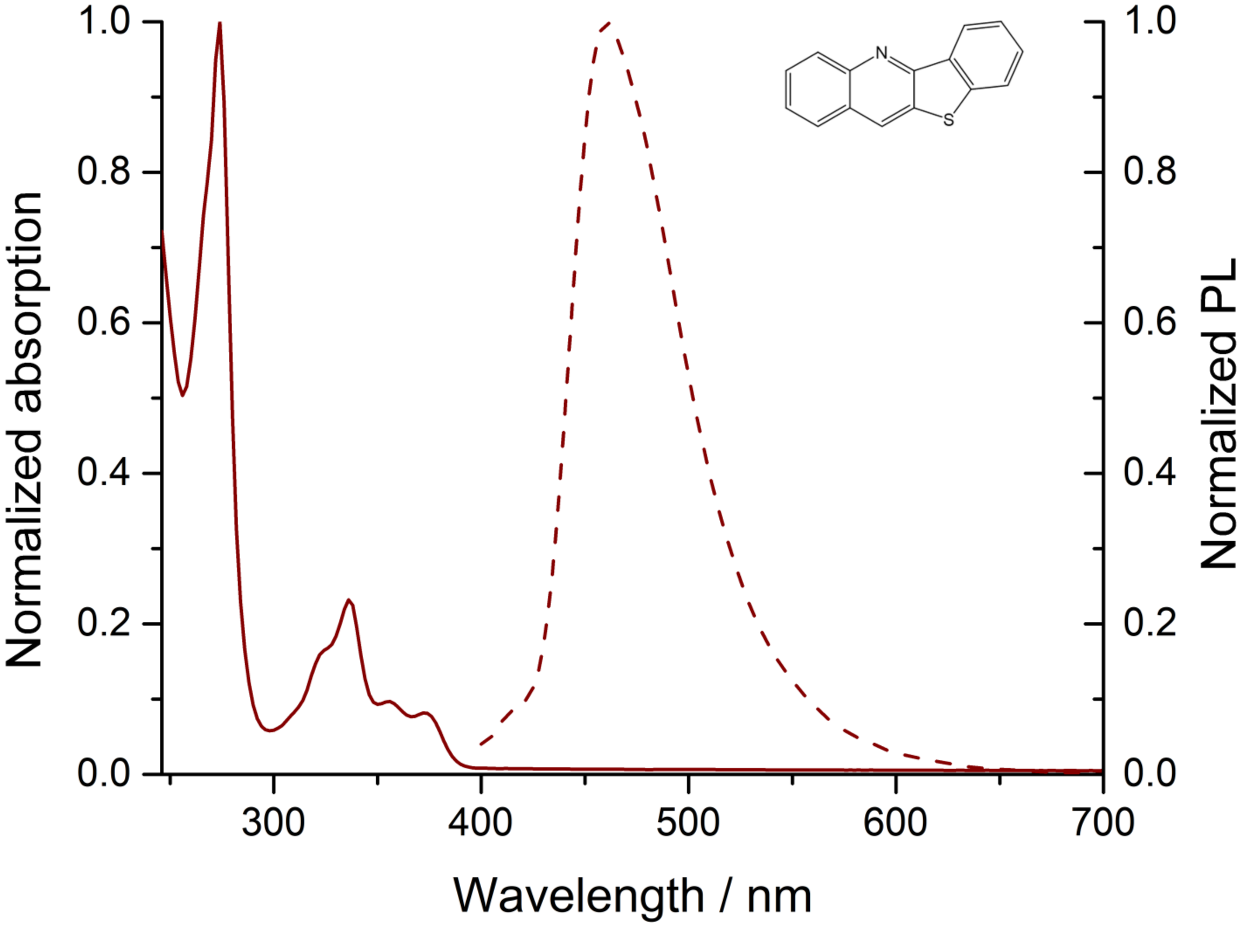

Figure 7: Normalized absorption and photoluminescence spectrum of compound **10f** in solution (50 µM in $CHCl_3$).

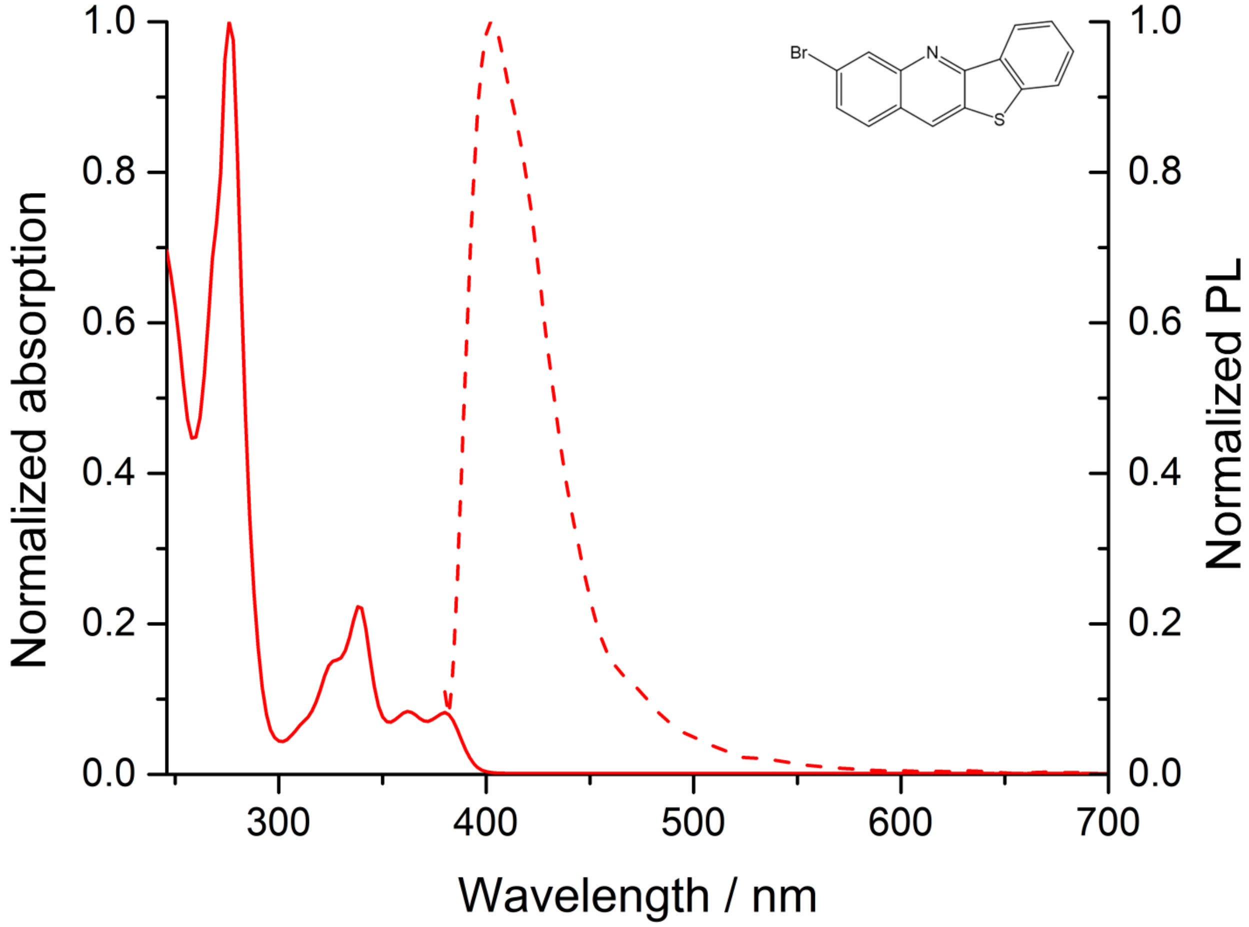

Figure 8: Normalized absorption and photoluminescence spectrum of compound **10g** in solution (50 µM in $CHCl_3$).

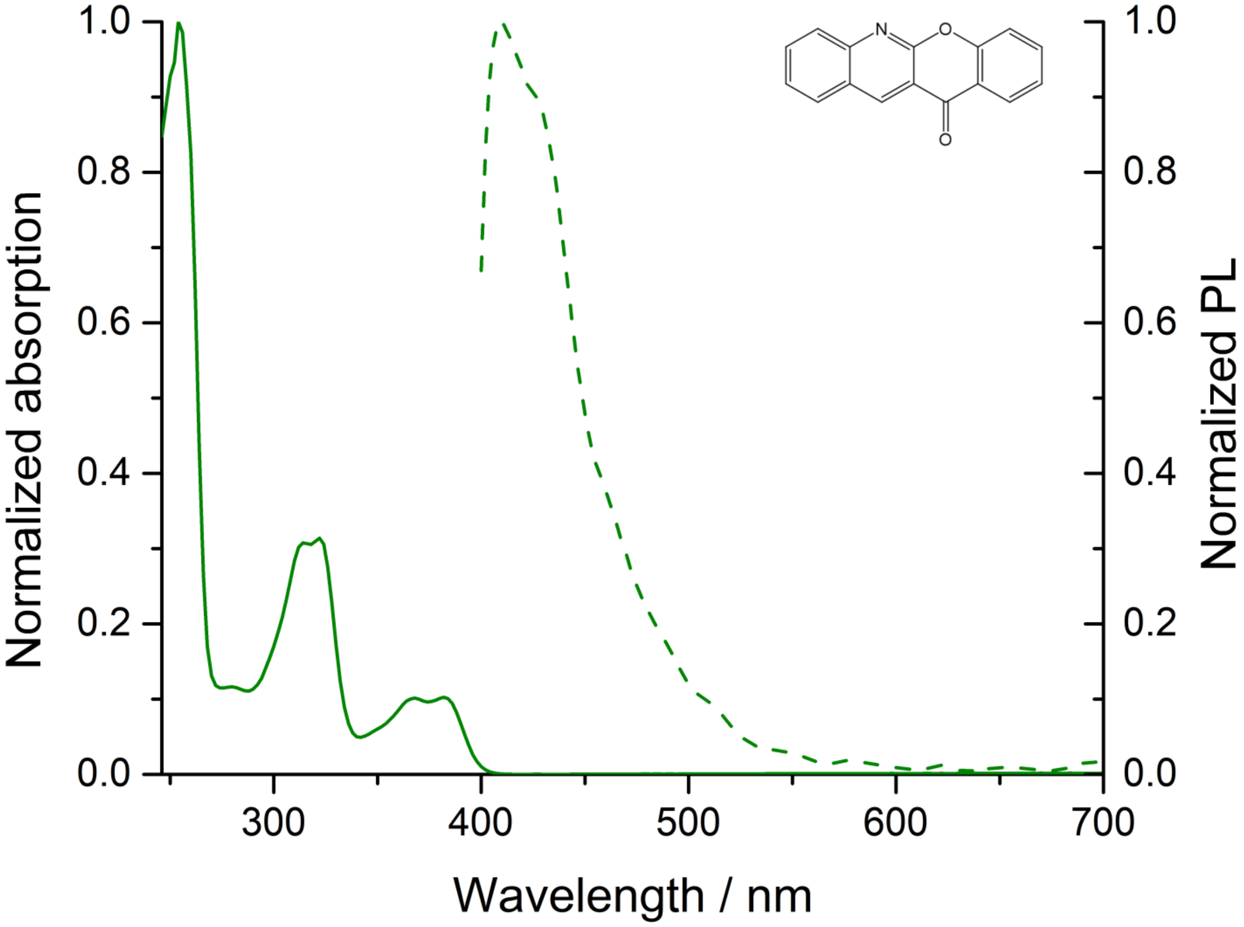

Figure 9: Normalized absorption and photoluminescence spectrum of compound **10j** in solution (50 µM in $CHCl_3$).

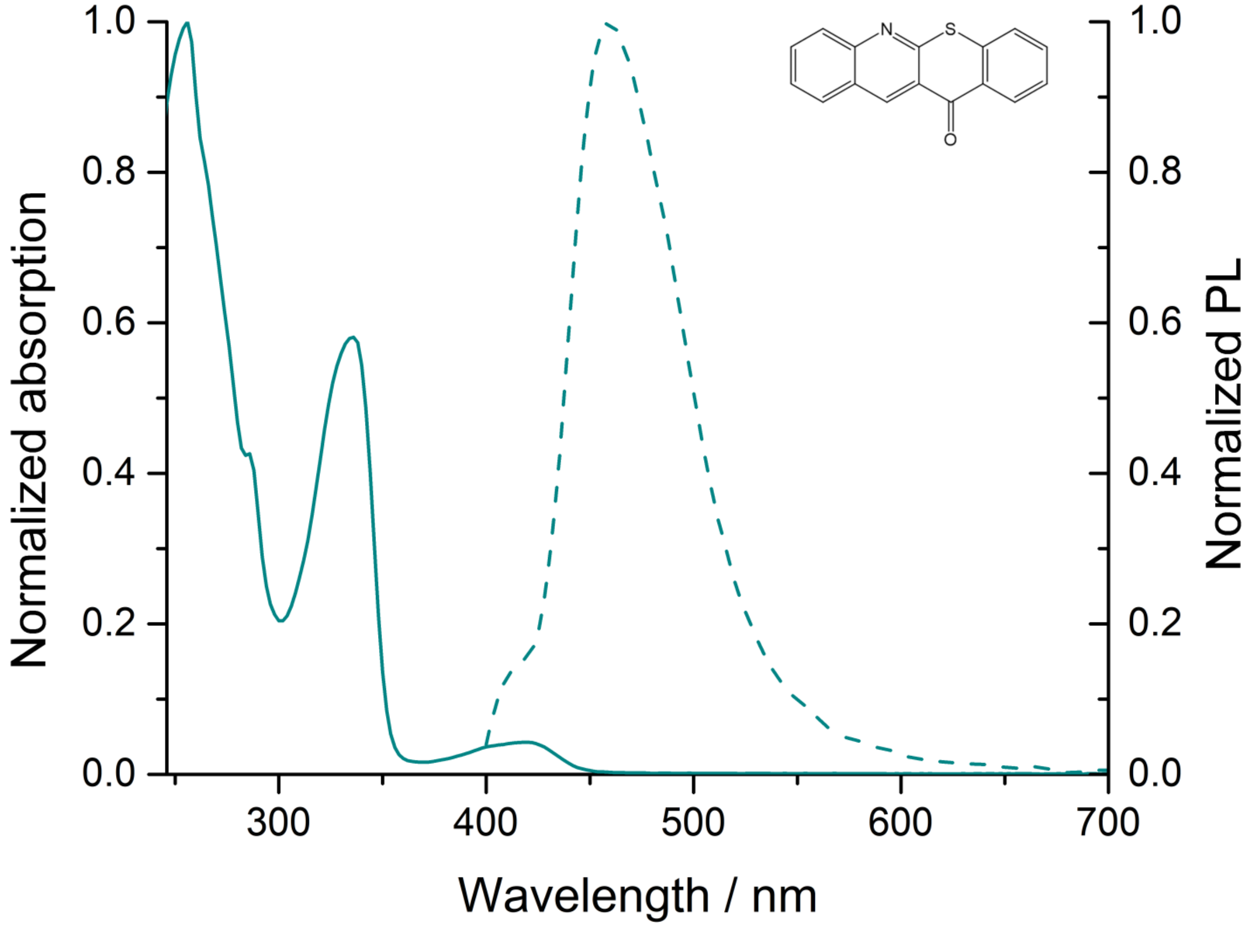

Figure 10: Normalized absorption and photoluminescence spectrum of compound **10k** in solution (50 µM in $CHCl_3$).

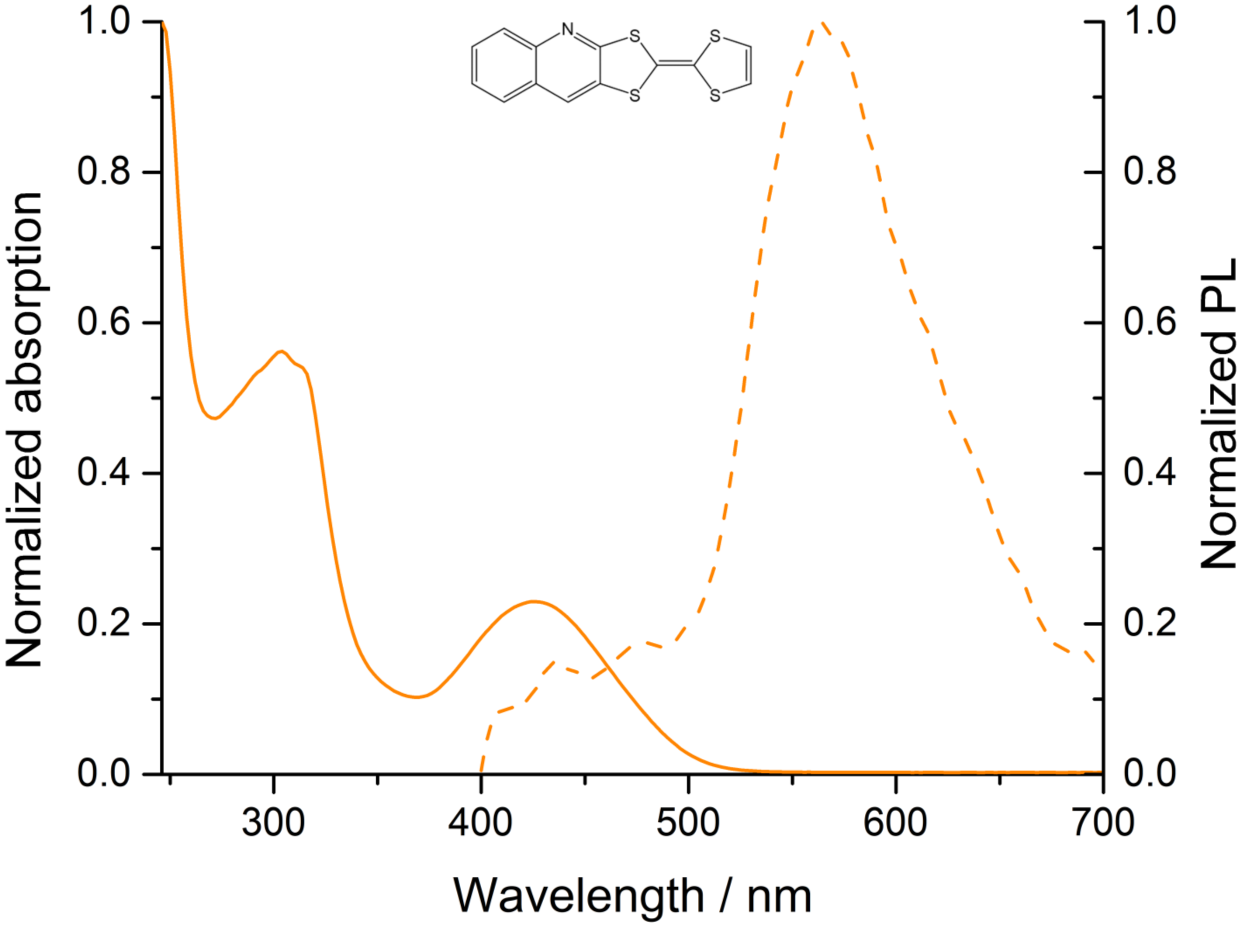

Figure 11: Normalized absorption and photoluminescence spectrum of compound **10m** in solution (50 µM in $CHCl_3$).

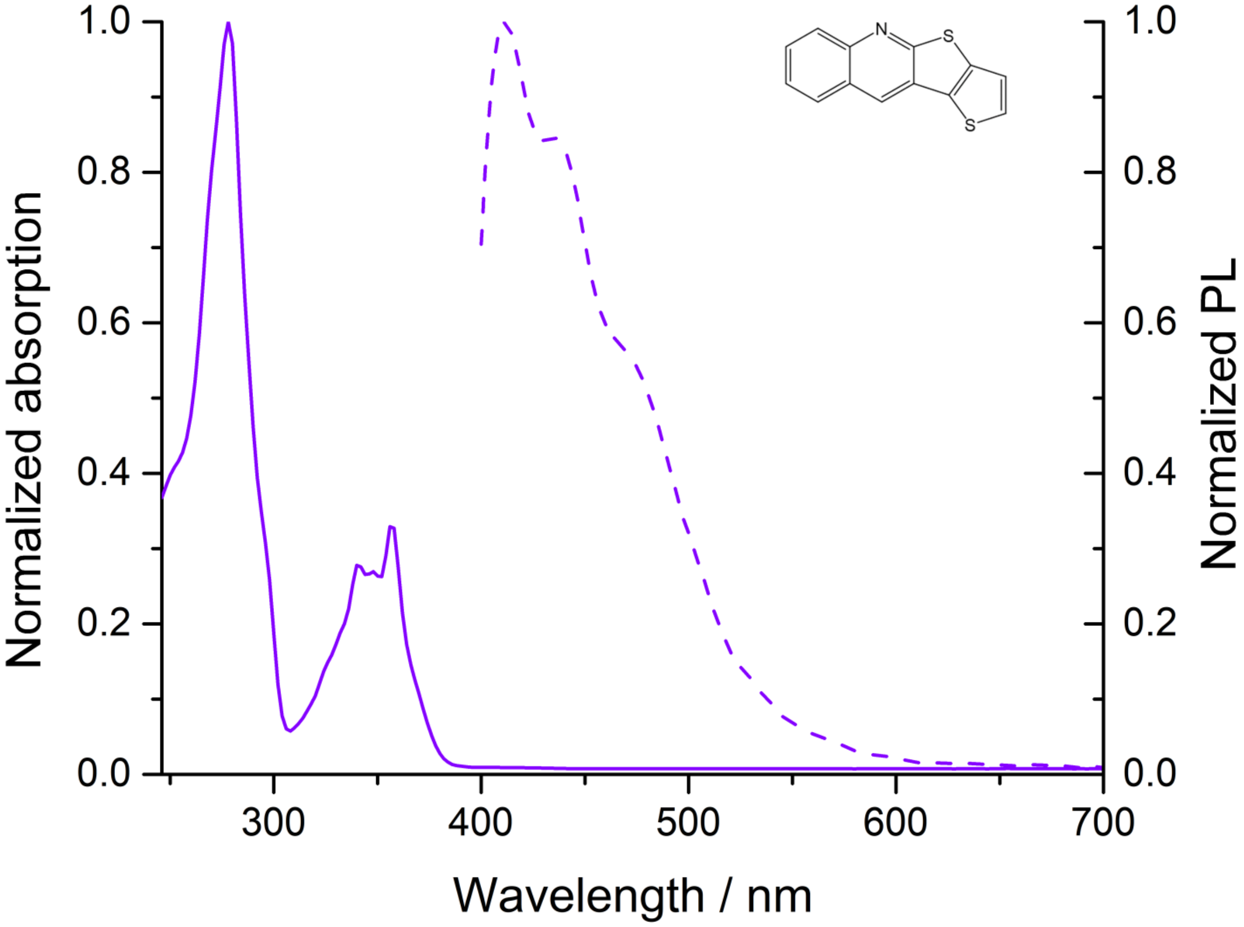

Figure 12: Normalized absorption and photoluminescence spectrum of compound **10n** in solution (50 µM in $CHCl_3$).

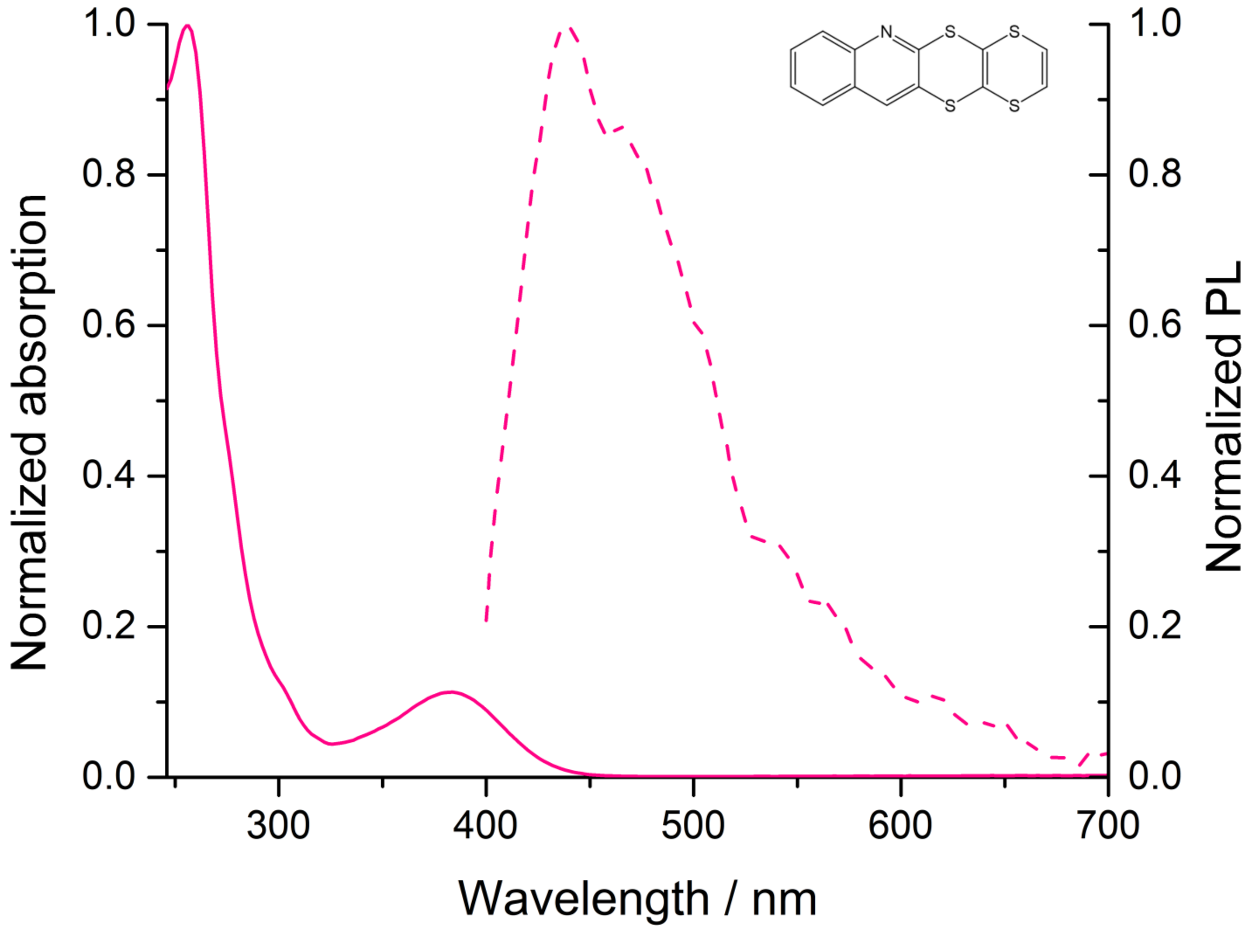

Figure 13: Normalized absorption and photoluminescence spectrum of compound **10o** in solution (50 µM in $CHCl_3$).

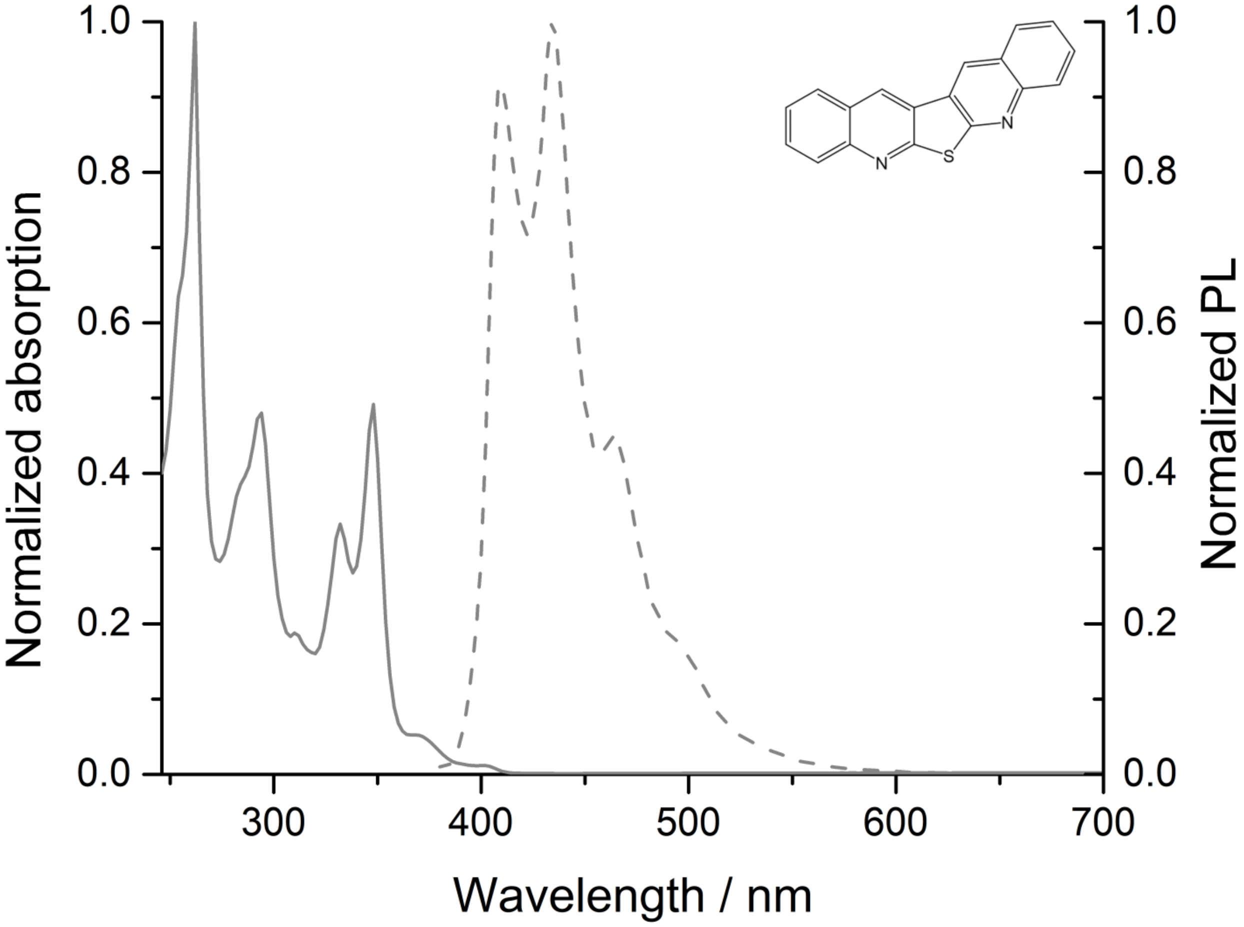

Figure 14: Normalized absorption and photoluminescence spectrum of compound **14** in solution (50 µM in $CHCl_3$).

Tauc plots

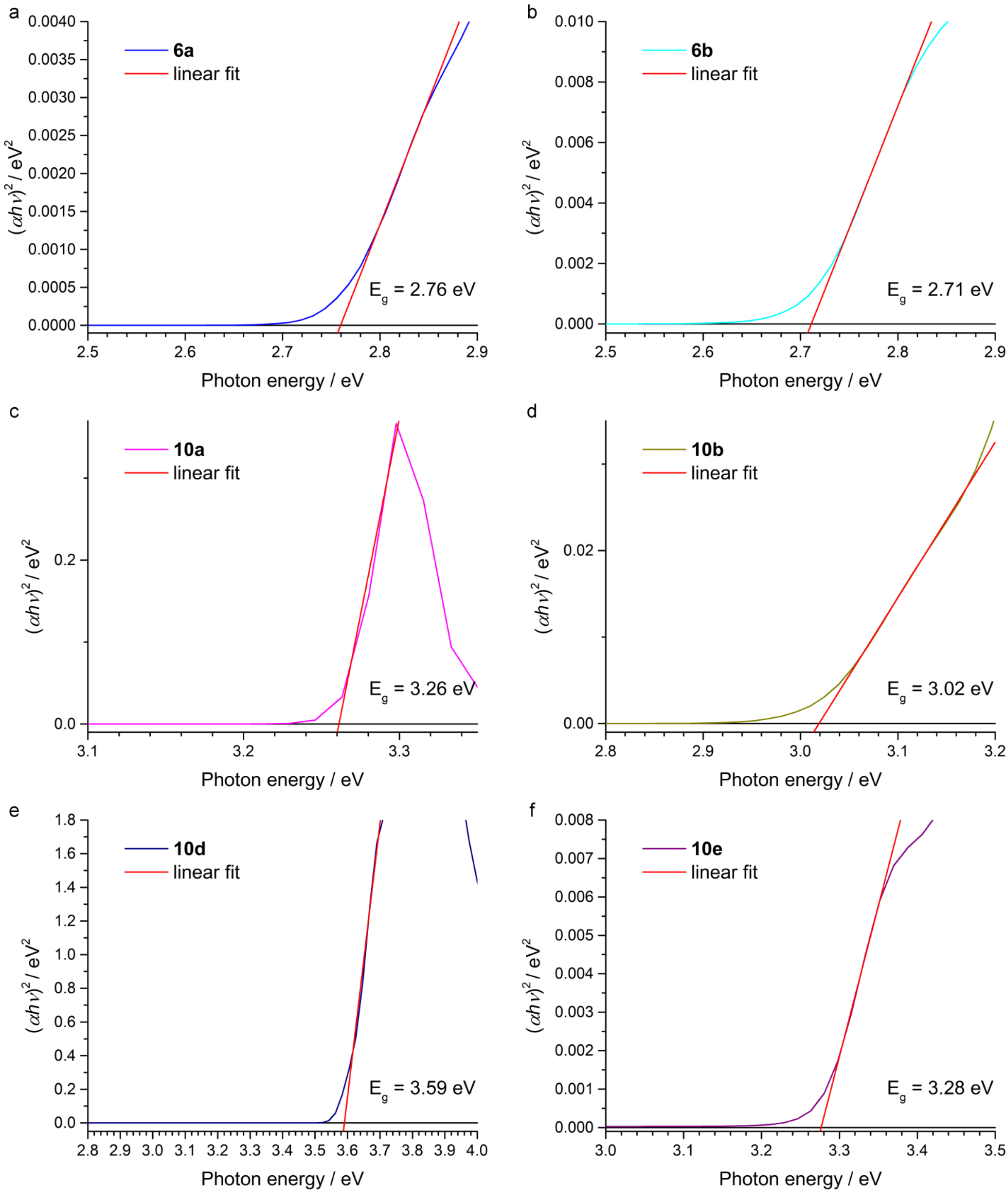

Figure 15: Tauc plots generated from optical absorption spectra of selected condensed N-heterocycles and linear fits for direct band gaps (red). The energy of the bandgap is shown in each graph on the bottom right.

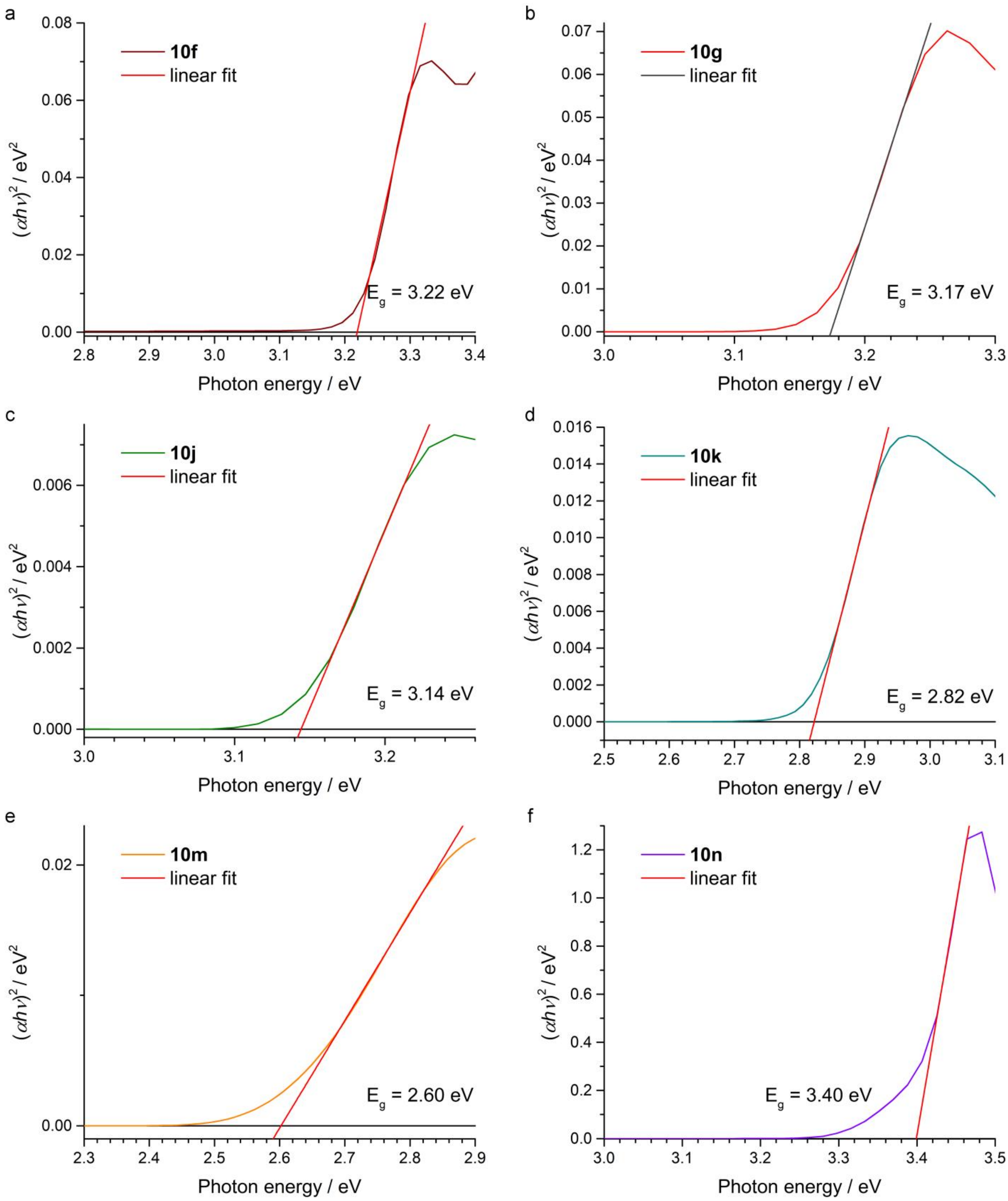

Figure 16: Tauc plots generated from optical absorption spectra of selected condensed N-heterocycles and linear fits for direct band gaps (red, except (b) in grey). The energy of the bandgap is shown in each graph on the bottom right.

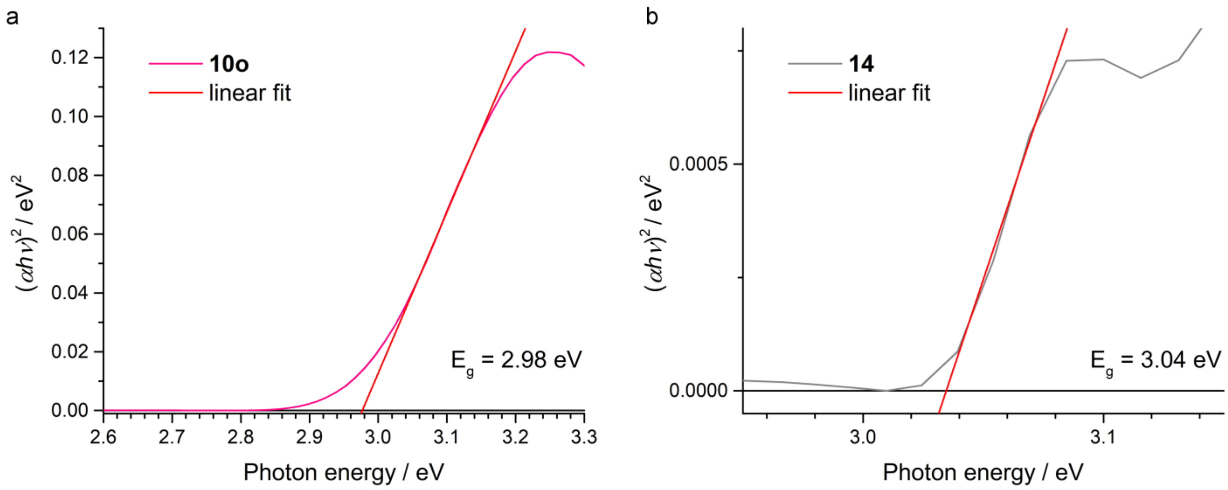

Figure 17: Tauc plots generated from optical absorption spectra of selected condensed N-heterocycles and linear fits for direct band gaps (red). The energy of the bandgap is shown in each graph on the bottom right.

Photoluminescence quantum yield

We measured the photoluminescence quantum yield PLQY using a PicoQuant FluoTime 300 spectrometer and the software *easytau*.

Compound	PLQY / %
6b	37.32
10b	26.35
6a	15.31
10a	4.89
14	3.39
10k	2.13
10n	1.56
10e	1.13
10f	0.87
10g	0.39
10j	0.17
10d	0
10m	0
10o	0

Time-correlated single photon counting

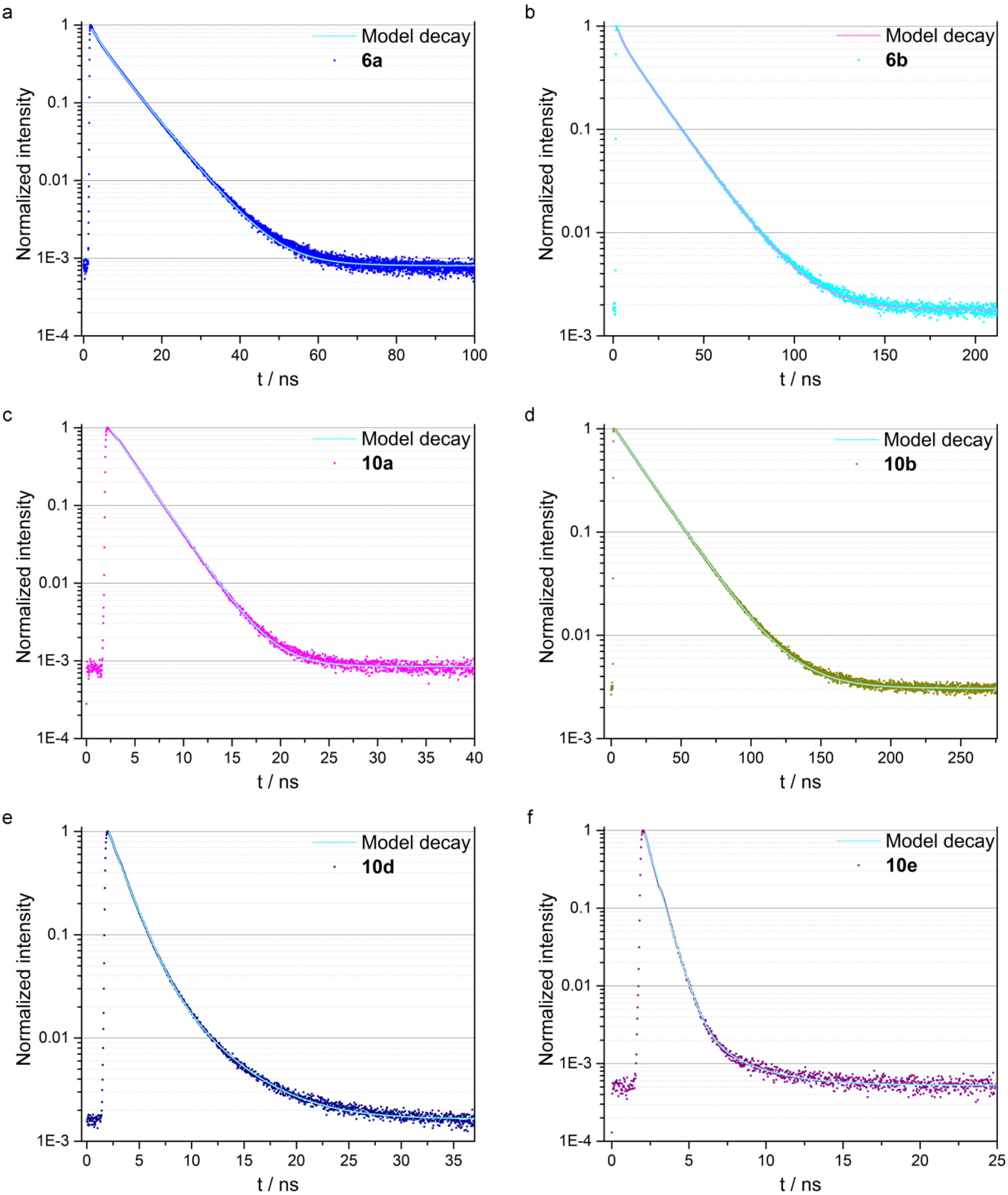

Figure 18: PL decay of selected condensed N-heterocycles excited at 378 nm and measured at the corresponding maxima of the PL emissions. All samples were measured in solution (50 µM in $CHCl_3$). Experimental decay is shown in dots and the corresponding mono- or bi-exponential fit of the decay as light cyan line.

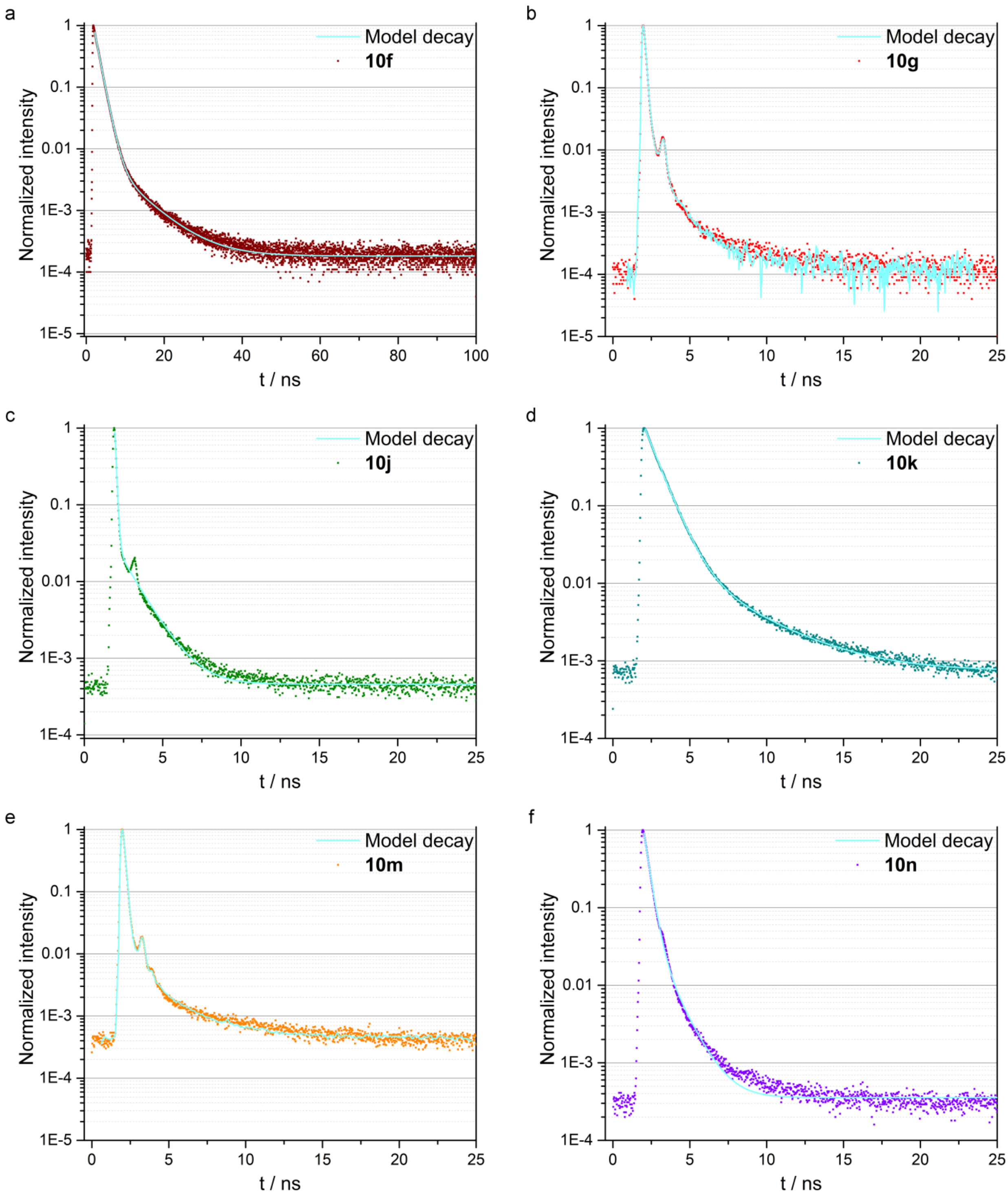

Figure 19: PL decay of selected condensed N-heterocycles excited at 378 nm and measured at the corresponding maxima of the PL emissions. All samples were measured in solution (50 µM in $CHCl_3$). Experimental decay is shown in dots and the corresponding mono- or bi-exponential fit of the decay as light cyan line. The additional peak in the decay is due to the instrument response function that can be observed for fast decays (b, c, e)

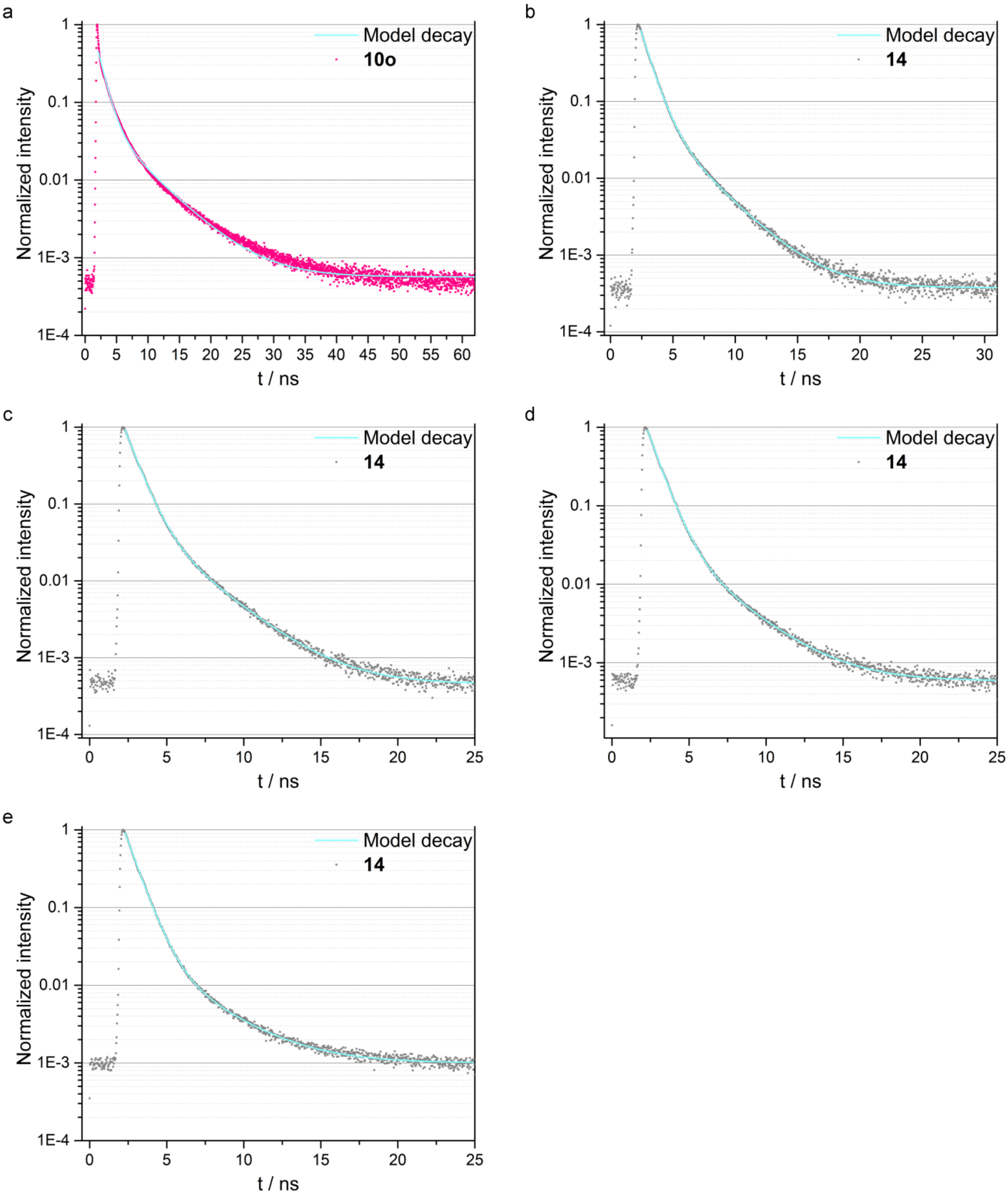

Figure 20: PL decay of selected condensed N-heterocycles excited at 378 nm and measured at the corresponding maxima of the PL emissions. All samples were measured in solution (50 µM in $CHCl_3$). Experimental decay is shown in dots and the corresponding mono- or bi-exponential fit of the decay as light cyan line. For compound 14 the decay traces have been recorded at different emission wavelength of the four maxima in the PL spectrum: (b) 410 nm, (c) 434 nm, (d) 464 nm, (e) 494 nm.

Table 1: PL decay times of compounds shown above. The given errors are uncertainties from the fit and hence do not reflect the real time-resolution of the setup. The latter is limited by the laser pulse duration of around 100 ps.

		τ / ns	error / ns	fractional intensity / %
6a	τ_1	7.08	±0.02	75.7
	τ_2	2.61	±0.06	24.3
6b	τ_1	17.51	±0.05	80.3
	τ_2	3.2	±0.2	19.7
10a	τ_1	2.414	±0.007	100
10b	τ_1	22.00	±0.06	100
10d	τ_1	1.478	±0.004	92.8
	τ_2	4.27	±0.03	7.2
10e	τ_1	2.7	±0.1	0.6
	τ_2	0.615	±0.002	99.4
10f	τ_1	7.2	±0.1	1.1
	τ_2	1.305	±0.005	98.9
10g	τ_1	1.10	±0.09	0.2
	τ_2	0.0670	±0.0008	99.8
10j	τ_1	1.23	±0.03	3.3
	τ_2	0.085	±0.002	96.7
10k	τ_1	3.59	±0.04	2.6
	τ_2	0.849	±0.002	97.4
10m	τ_1	2.1	±0.1	0.2
	τ_2	0.1225	±0.0007	99.8
10n	τ_1	1.06	±0.02	5.9
	τ_2	0.315	±0.003	94.1

10o	τ_1	5.5	±0.1	12.2
	τ_2	1.19	±0.02	87.8
14 ($\lambda_{em.}$ = 410 nm)	τ_1	2.72	±0.02	8.6
	τ_2	0.789	±0.003	91.4
14 ($\lambda_{em.}$ = 434 nm)	τ_1	2.71	±0.02	7.7
	τ_2	0.791	±0.003	92.3
14 ($\lambda_{em.}$ = 464 nm)	τ_1	2.74	±0.02	5.1
	τ_2	0.776	±0.002	94.9
14 ($\lambda_{em.}$ = 494 nm)	τ_1	3.03	±0.03	3.5
	τ_2	0.767	±0.002	96.5

Cyclic voltammetry and energy levels of HOMO and LUMO

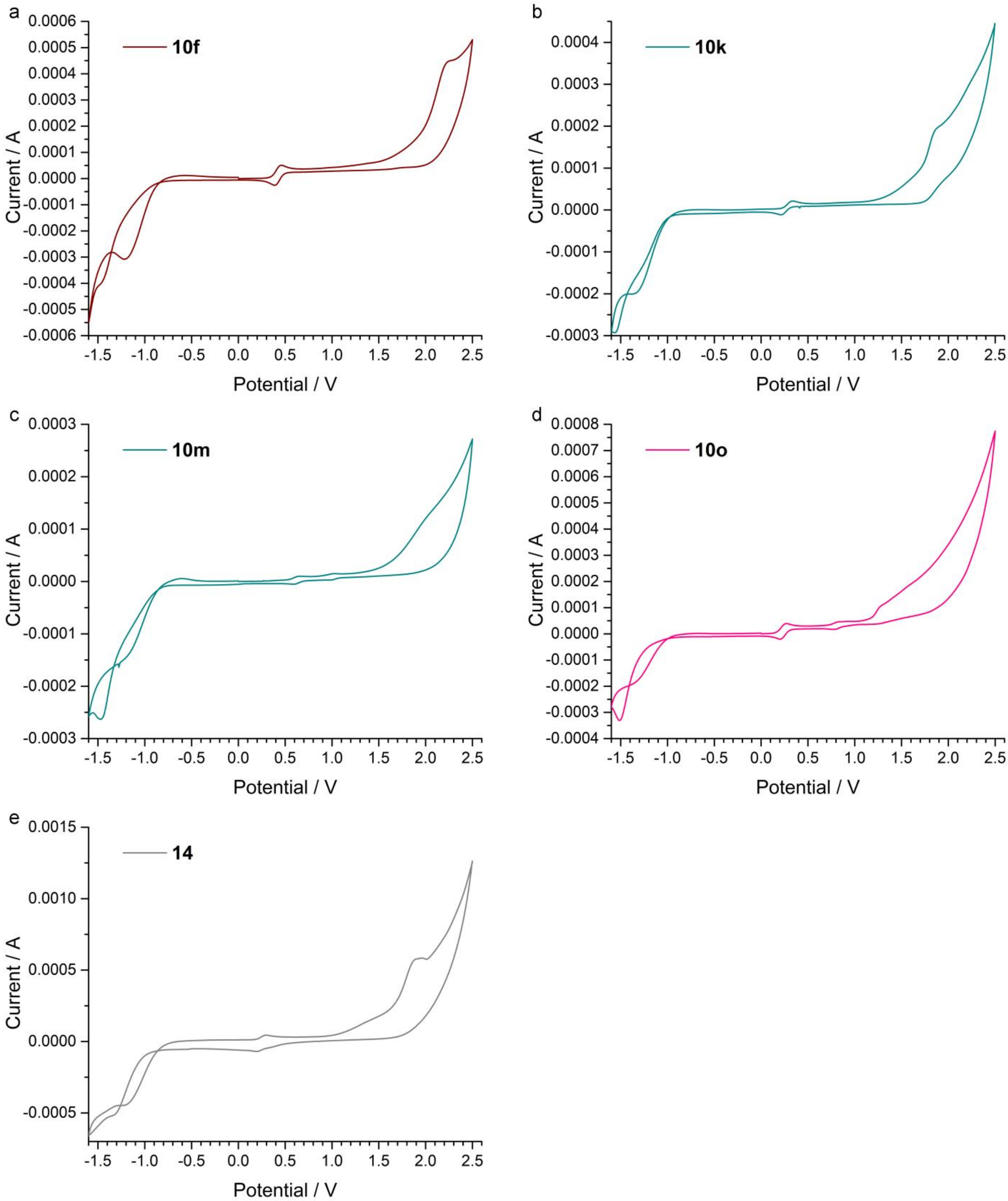

Figure 21: CV measurements of compounds **10f**, **10k**, **10m**, **10o**, and **14**. All samples were measured according to the procedure described before. Below the potential of −1.0 V the redox behavior of the electrolyte can be observed. An external reference was used for **10m** due to the overlap of the signals.

Table 2: CV measurements of the compounds and the corresponding optical determined HOMO-LUMO gaps lead to the exact positions of the HOMO and LUMO of the selected condensed N-heterocycles.

	HOMO / eV	LUMO / eV

10f	−6.3	−3.1
10k	−6.3	−3.4
10m	−4.9	−2.3
10o	−5.3	−2.3
14	−6.2	−3.2